Advances in MOEMS Technologies for high quality imaging systems

Harald Schenk[a,b], Michael Wagner[a], Jan Grahmann[a], André Merten[a]
[a]Fraunhofer Institute for Photonic Microsystems, Dresden, Germany; [b]Brandenburg University of Technology Cottbus-Senftenberg, Cottbus, Germany

ABSTRACT

An overview of advances in MOEMS devices and technologies for high quality imaging systems is provided. A particular focus is laid on recent technological further developments possibly opening gateways to unprecedented device and system functionality by e. g.: increase of pixel count towards higher parallel operation, decrease of the mirror pitch in large arrays towards applications like high-performance holography, novel technologies for higher operation bandwidth, increase of aperture size for scanning applications like LIDAR, integration of high reflection coatings for processing of multi Watt laser radiation for marking and engraving, and phased arrays for high speed laser beam steering.

Keywords: MEMS, MOEMS, scanner, micro mirror, micro scanner, spatial light modulator, micro mirror array, marking, engraving, lithography, LIDAR

1. INTRODUCTION

MOEMS – the integration of micro-optics and MEMS – has become an enabling technology in a wide range of high-quality imaging applications. Microscopy, medical imaging, 3D ranging, laser marking, image projection and, last but not least, lithography profit from one or more key features of MOEMS devices. These key features comprise large operation bandwidth, highly parallel operation, high level of reproducibility and small device dimensions. MOEMS technology is provider of a wide range of groundbreaking solutions to complex optical problems: Highly accurate spatial and temporal modulation of an electromagnetic field's amplitude and phase allows us e. g. to correct static and dynamic image distortions or to generate arbitrary illumination patterns including illumination angle control.

The toolkit of MOEMS modulator technologies has reached a remarkable level of versatility. The spectrum of components covers scanning mirrors for 1D [1] and 2D resonant [2] as well as quasi-static deflection [3], [4] with apertures in the mm-range, piston-type scanners for path length modulation of several 100 µm [5], scanning gratings for wavelengths from DUV up to the mid infrared [6], miniaturized tunable lenses [7], high-performance deformable mirrors [8] as well as micro mirror arrays with up to millions of digital [9] or analog deflectable pixels [10], [11]. The spectrum of fabrication technologies is based on surface and bulk micromachining, and on monolithic or hybrid integration of MOEMS and CMOS.

As a whole, these base technologies intrinsically provide key features like high integration, high pixel count, high switching/operation speed due to low masses/moment of inertia as well as high structural and material homogeneity. To address special and highly challenging requirements application-specific process solutions were and are being developed. Such challenging requirements are in particular highly accurate deflection control, optical very high-quality surfaces including high planarity, stress minimized high reflective optical coatings to withstand high-energy radiation exposure, deflections with multiple degrees of freedom as well as very small pixel sizes down to dimensions enabling phased arrays or even subwavelength modulation.

In the following, status and further developments in MOEMS technology addressing such challenging requirements are described by means of concrete device examples from the fields i) light deflection and scanning (section 2) and ii) spatial light modulation (section 3). Focus is laid on device properties and features of particular device elements which determine the properties as optical modulator for high-quality imaging systems.

Optical Microlithography XXXI, edited by Jongwook Kye, Proc. of SPIE Vol. 10587,
1058703 · © 2018 SPIE · CCC code: 0277-786X/18/$18 · doi: 10.1117/12.2297399

2. SCANNING MICRO MIRRORS FOR LINE FREQUENCIES UP TO THE KHZ-RANGE

For scanning applications various light deflection devices are available. Precision-engineered galvanometers, polygons, and piezo scanners as well as acousto and electro optical modulators offer a wide range of frequencies, deflection angles and position accuracy levels. Scanning micro mirror technology has proven to significantly add to the accessible bandwidth of technical parameters and in particular offers combinations of parameters not possible with other scanner technologies. Acousto and electro optical modulators offer the highest deflection frequencies of up to several 100 MHz and – in combination with the possibility to generate spots of small diameter – a high pixel rate. Yet, deflection angles of up to a few 10 mrad are low and level of possible compactness is highly restricted. The partially high system complexity limits the range of applicability. In comparison to acousto and electro optical modulators precision engineered piezo scanners, galvanometers and polygons provide significant lower operation frequencies, typically up to a few kHz, but offer larger deflection angles of up to several 10 degrees.

Apart from the fact that MEMS scanners offer the lowest fabrication cost for high volumes, making them first choice for consumer and automotive applications, their very high compactness and the possibility for deflection frequencies up to the 100 kHz range in combination with deflection angles of several degrees up to several ten degrees make them attractive also for a large variety of special applications. The advantage of high compactness becomes particularly obvious when two-dimensional deflection is required.

The basic set-up of micro scanning mirrors is defined by a rectangular or elliptical plate suspended by two torsional springs and a means for driving. For that, various electrostatic, electromagnetic and piezoelectric mechanisms are being deployed. Figure 1a shows an example of a 1D scanner excited by an electrostatic comb drive.

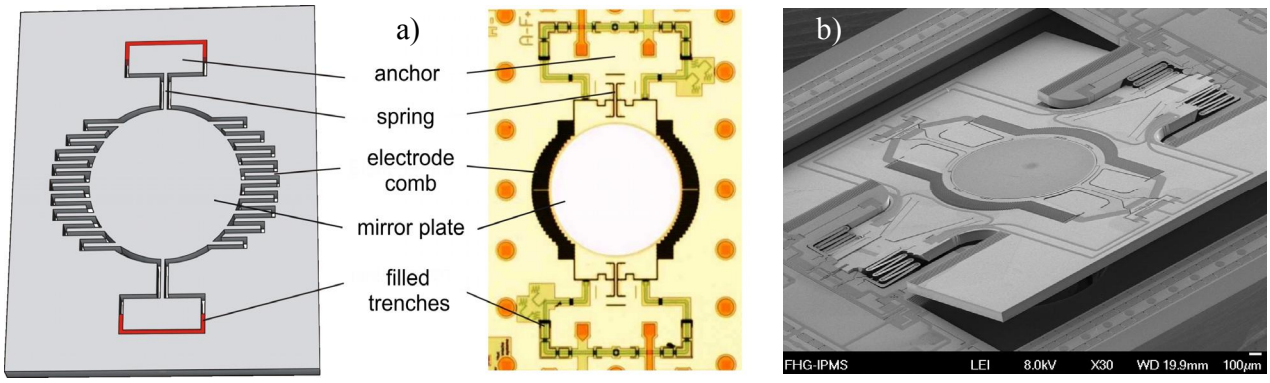

Figure 1. a) Left: principal set-up of a 1D micro scanner with mirror plate and torsional springs. Also shown is the electrode comb for driving. Right: micrograph of a 1D scanner with electrode comb drive. b) SEM image of a 2D micro scanner.

Extension towards 2D deflection is based on a serial combination of two 1D scanners or on a two-dimensional, gimbal-like suspension of the mirror plate as shown exemplarily in Figure 1b.

The number of spots which can be resolved by a particular micro mirror with a total optical scan angle Θ and mirror plate diameter D can be estimated by application of the Rayleigh criterion:

$$N = \frac{\Theta D}{a_f \lambda} \tag{1}$$

a_f is the aperture factor and λ the wavelength of the collimated laser beam.

This approach allows for an approximate comparison of the achievable spot number of different micro scanning mirrors. For a more detailed comparison further properties, in particular the mirror plate planarity, would have to be taken into account - an issue which will be addressed in section 2.1.

For reasons of mechanical stability and to keep the inertia-induced mirror plate deformation within an acceptable range, the diameter D of the mirror plate is typically in the range of 1 - 2 mm and ranges up to a few mm.

The rate at which pixels can be written is high for resonantly driven scanners and significantly lower when the scanners are operated quasistatic. In the latter case, a total optical scan angle of 20°, typically, for scan frequencies of a few 100 Hz are achieved for a mirror plate diameter of typically 1 - 2 mm (compare e. g. [3]). The limitation with respect to deflection angle, operation and switching speed, respectively, is given by the available driving force to control the deflection. Taking into account the huge efforts in development of scanner driving mechanisms based on virtually every physical force, it can be expected that only minor optimization will be achieved in the future if not the general architecture of MOEMS devices for deflection and beam steering is reconsidered (see e. g. section 2.4).

In case of resonant driving deflection amplitude profits from enhancement proportional to the quality factor. Thus, limits for mirror plate dimensions and scan frequency are not limited by the available driving force but by the mechanical load in the springs and the inertia-induced mirror plate deformation which degrades optical quality.

Figure 2 compares selected quasistatic and resonant micro scanning mirrors by means of the achievable pixel rate, the line rate and the number of resolvable pixels (Eq. 1). Please note that the optical quality of the mirror surface and in particular the mirror planarity was not taken into account. Depending on the wavelength and the particular optical quality requirements of an application the actual limits might thus be lower than indicated by the values displayed in Figure 2. The pixel rate was calculated assuming that the scanner is writing pixels in a bidirectional manner. Thus, the pixel rate corresponds to twice the resonance frequency, which is equal to the line rate, times the number of resolvable spots. The latter one was estimated according to equation (1) for a wavelength of 650 nm and is displayed in Figure 2 as the number of pixels. Note, that for the quasistatic scanners also twice the resonance frequency was applied for the calculation of the pixel rate. In reality, the maximum usable frequency depends on the required trajectory accuracy and can easily be less than half the resonance frequency.

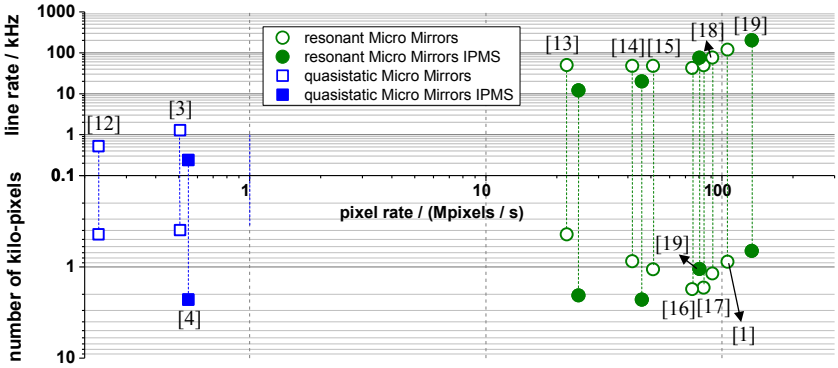

Figure 2. Comparison of selected quasistatic and resonant micro scanning mirrors. In case of resonant scanners focus is laid on high frequency devices. Note that for very high frequencies large deflection angles may require operation at reduced pressure.

2.1 Mirror planarity

In particular for high frequency large angle scanning use of "thick" silicon mirror plates is standard. Such plates provide sufficient bending stiffness to keep static deformation induced by thin metallic coatings considerably low. For example, radius of curvature can easily exceed 5 m and can range up to several 10 m for single crystalline mirror plates. A typical example for the latter is the fabrication by silicon on insulator technology with a plate thickness of 75 µm and an aluminum alloy layer of 50 nm with protective coating.

When operated inertial forces deform the mirror plate resulting in a degradation of its optical quality. The deformation, characterized by the surface error which is linearly increasing with scan angle Θ, is proportional to the square of the operating frequency f and proportional to the fifth power of the mirror diameter D [20]. By means of the modulation transfer function (MTF) the effect of the mechanical deformation on the spot size quality and, thus, the resolution can be described.

Several efforts were undertaken to improve the dynamic mirror planarity for a given parameter set of Θ, D and f. The obvious measure is to increase the thickness of the mirror plate. However, in many micro scanner technologies

fabrication issues do not allow realization of plate thicknesses significantly beyond 100 µm. Another approach, developed by our group, aims at suitable design measures to reduce the plate's deformation amplitude: The mechanical restoring torque is not only provided by the central springs but also by additional springs distributed along the plate's rim. This "distributed spring" approach allows to reduce the dynamic plate deformation and results in an enhancement of spot resolution of a factor of typically 3 (compare Figure 3) when compared to a similar mirror with standard design (i. e. two central springs).

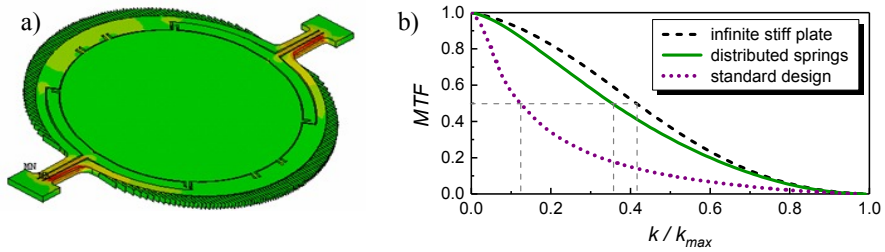

Figure 3. a) Finite element model of a micro mirror (f = 17 kHz, mirror plate diameter D = 1 mm) with optimized spring configuration comprising 8 springs distributed along the periphery of the circular mirror plate. b) Calculated modulation transfer function (MTF) for the mirror with distributed springs in comparison to one of the same parameters but with standard spring design. The MTFs were calculated at a mechanical deflection angle of 10° during resonant operation. Further parameters: λ = 633 nm, plate thickness: 30 µm.

2.2 Irradiation resistance and high laser power operation

High laser power operation in particular requires a high reflection coating of the mirror plate. Due to the small mirror plate thickness, typically in the range of 30 - 100 µm, there are high demands on the coating process and the coating design to achieve acceptable optical flat mirrors.

Table 1 shows the reflectivity of some hybrid coatings consisting of $(Ta_2O_5/SiO_2)^n$-layers on top of an AlSiTi metal layer. Figure 4 shows the measured reflectivity of the stack optimized for 450 nm.

Table 1. Experimentally determined reflectivity of three example coatings including a broad band coating for 450 - 750 nm.

wavelength	450 nm	450 – 700 nm	950 nm
Simulation	99.1 %	95.8 %	99.2 %
measurement	(98.6 ± 0.9) %	(95.5 ± 1.4) %	(99.4 ± 0.6) %

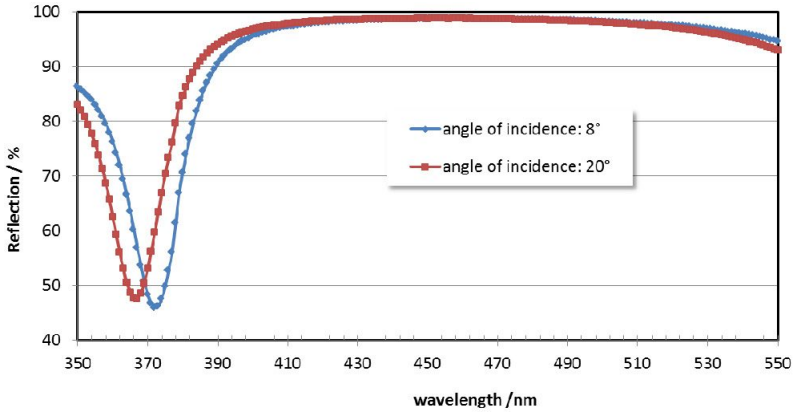

Figure 4. Experimentally determined reflectivity of a hybrid high-reflective coating at two different angles of incidence. The coating consists of a $(Ta_2O_5/SiO_2)^n$-layer stack on top of an AlSiTi metal layer.

In particular for very high reflection coefficients a larger number of the dielectric stacks needs to be deposited. On top of stress compensating measures for the coating layers the symmetric deposition on both sides of the mirror plate is a viable way to reduce static mirror deformation. The example of Figure 5 depicts a mirror with two-sided, stress and temperature compensated Bragg coating. The reflection coefficient is larger than 99.9 % at 532 nm. Despite the multiple dielectric stacks radius of curvature R could be kept larger than 5 m.

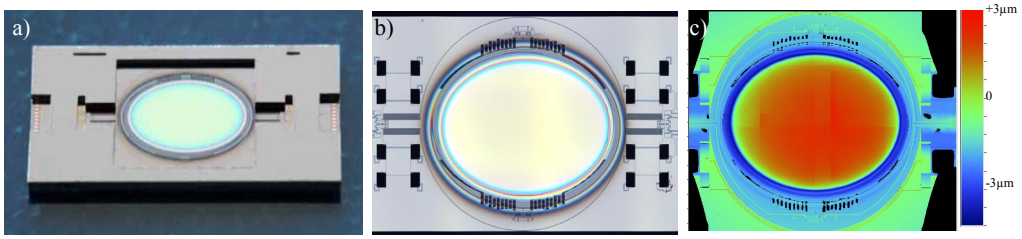

Figure 5. a) 2D MEMS scanner with large aperture size (elliptical, 5 mm/7.1 mm) and dielectric high-reflection Bragg coating on the 75 µm thick silicon plate. View: top side. b) Backside of the chip. A symmetrical coating was deposited on both sides of the suspended silicon plate. c) White Light Interferometry measurement result yielding R > 5 m.

Scanners of this type were exposed to high power ps-laser irradiation with an average power of up to 20 W (beam diameter 2 mm $1/e^2$, repetition rate 20 - 35 kHz) for 1 h with a total of 65 million pulses. None of the 10 tested samples showed any failure. During irradiation temperature rise of the mirror plate was 12 K, only.

2.3 Position read-out and control

Accurate position read-out allows for data synchronization, amplitude control of resonant scanners and trajectory control of quasistatic scanners. Our group developed both, optical hybrid and integrated position read-out. Optical hybrid read-out requires at least two laser beams and two photo diodes and is easy to implement. However, for practical reasons this variant is limited to resonant scanners and 1D deflection. Integrated position sensors offer accurate position control for all scanner types and in particular can also be applied for control of static deflection. The sensor element is e. g. realized by a thin, embedded piezoresistive layer in the anchor region. With a particular design of such a sensor element a sensitivity of 100 mV/V at a current of 100 µA and a signal to noise ratio of 965 at a resonant deflection angle of 10° has been demonstrated by us. For a quasistatic scanner a similar sensor element was designed for closed loop trajectory control to provide highly linear scans. With a position accuracy of ±5 m° and a mechanical deflection angle of ±7° a total of 1400 positions were resolved.

2.4 Increase of optical aperture and scan frequency

Dynamical deformation as described in section 2.1 limits mirror aperture size in particular for high scan frequencies significantly. For a 2 mm diameter micro scanning mirror providing an optical scan range of 40° the scan frequency will typically be not much higher than 5 - 10 kHz depending on the operation wavelength and on surface quality requirements. A further restriction is based on the mechanical stress in the torsional hinges which will exceed the acceptable limits with increasing scan frequency, deflection angle and, in particular, with aperture size.

Two key developments provide a way towards large-aperture, high-frequency scanning: a) synchronization of multiple micro scanning mirrors and b) deployment of phased arrays.

Examples for synchronized micro scanning mirrors with very high effective aperture sizes of up to 776 mm² are shown in Figure 6.

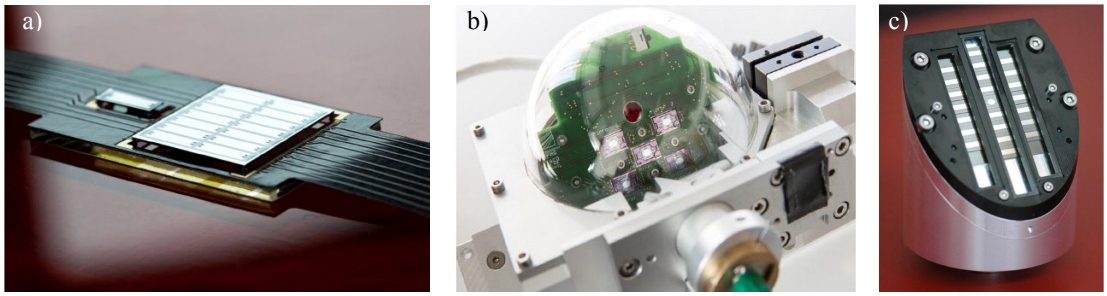

Figure 6. Examples of synchronized micro scanning mirrors for large effective optical apertures. a) Array of 2 x 7 1D resonantly driven scanners with an optical scan range of 60° at 250 Hz and an effective optical aperture of 334 mm² (optical fill factor 80 %). The separately mounted mirror serves as sending mirror for a phase shift-based distance measurement application. b) Array of five 2D micro scanning mirrors with a 1.6 kHz resonantly driven fast axis and a quasistatic driven slow axis (0 – 50 Hz for closed loop controlled linear trajectory). Each of the 5 synchronized mirrors contributes with its elliptical aperture of 2.6 mm/3.6 mm to a total effective aperture size of up to 37 mm² (for the Time-of-Flight application one mirror is used as sending mirror). c) Assembly of 22 receiving 1D scanning mirrors with an aperture of 4.2 x 8.4 mm², each. The sending mirror in the middle has an elliptical aperture of 3.3 mm/3.6 mm. The mirrors are driven resonantly at 1.6 kHz and enable a maximum optical scan range of 80°.

Beam steering based on the optical phased array principle allows reducing mirror size drastically with the effect of reduced moment of inertia and thus increasing of scan and switching frequency, respectively. Recently, a MEMS optical phased array for optical beam steering and beam forming was presented by UCLA (compare Figure 7) where the resonance frequency of the individual mirrors is 310 kHz. The 1D array consists of 2.1 µm wide and 30 µm long micro mirror stripes (pitch 2.4 µm) each providing a piston-type deflection of up to 0.4 µm at 10 V. At a wavelength of 905 nm 256 spots can be resolved within an optical range of 22°. [21]

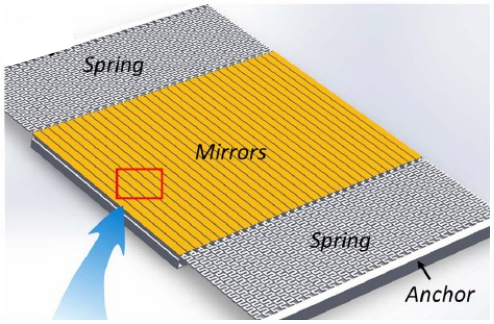

Figure 7. Schematic of the optical phased array [21].

3. MICRO MIRROR ARRAYS FOR PIXEL RATES UP TO THE MHZ-RANGE

Micro mirrors arrays consist of either a linear or a two-dimensional arrangement of individually deflectable mirror elements. Deflection is possible either between, typically two, fixed positions (digital) or in an analog manner.

The 2D digital mirror arrays of Texas Instruments are being used and investigated for a huge variety of applications in particular in the context of image generation. Each mirror corresponds to a pixel in the image area. One of the two stable mirror positions corresponds to “black” and the other one to “white”. The corresponding beamlet is switched by the individual mirror either towards the image plane or towards an absorber. The mirror device principle is independent on the wavelength and the coherence of the light source. Thus, it can be applied highly flexible for various illumination sources with wavelength from UV to infrared. Grey value generation relies on time-multiplexing.

Another principle for image generation makes use of the diffractive properties of an array. Here, the 1D or 2D device is acting as a programmable grating with locally addressable diffraction efficiency. An aperture stop in the Fourier-plane allows light of a given diffraction order only to pass through and to contribute to the image. Light from other diffraction orders is blocked. This principle can be applied to both digital and analog-operated mirror devices. In case of analog-operated mirrors a particular advantage of simultaneous grey value generation can be exploited (compare Figure 8). The analog deflection of the mirrors enables to vary between a highly efficient and very low efficient local grating structure. Thus, grey value generation is possible without time-multiplexing allowing for high grey value frame rates.

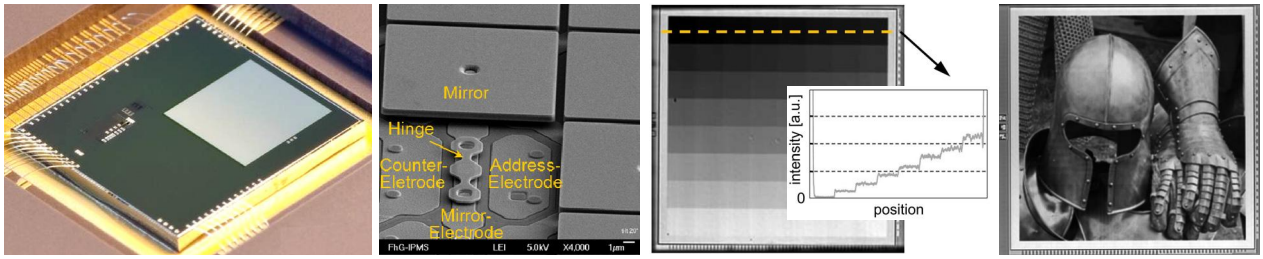

Figure 8. Analog addressable micro mirror array example of Fraunhofer IPMS. From left to right: Array with 256 x 256 micro mirrors with a pitch of 16 µm and an optical fill factor of 92 %. SEM picture with one mirror plate removed to reveal the two layer architecture (hinge layer and mirror layer). 8 x 8 grey scale patterns imaged at 680 nm - the intensity course of the 8 darkest grey values is shown in the inset. Generated grey scale image.

Table 2 displays the frame rates, the pixel rates and the array size of selected micro mirror array devices with high pixel count and high frame rate for advanced imaging.

Table 2. Comparison of selected micro mirror arrays for advanced imaging. For reasons of better comparability, the last column lists the pixel rate for 6 bit grey scaling. Note that Texas Instrument also offers a DMD chip for Ultra-HD resolution with 3840 x 2160 pixels [23].

Device	deflection	number of pixels	max. frame rate	max. pixel rate	pixel rate for 6 bit grey scaling
DMD / Texas Instruments [22]	digital	1920 x 1080	48 kHz	$1.1 \cdot 10^{11}$/s	$1.6 \cdot 10^{9}$/s
GLV / Silicon Light Machines [10]	analog	8192 x 1	250 kHz	$2.0 \cdot 10^{9}$/s	$2.0 \cdot 10^{7}$/s
2D ASLM / IPMS	analog	2048 x 512	2 kHz	$2.1 \cdot 10^{9}$/s	$2.1 \cdot 10^{9}$/s
1D ASLM / IPMS [11]	analog	8192 x 1	1.2 MHz	$1.0 \cdot 10^{10}$/s	$1.0 \cdot 10^{10}$/s

A third class of micro mirror arrays comprises mirrors which can be analog-deflected, preferably in two dimensions (tip-tilt), allowing to arbitrarily deflect beamlets. Such highly versatile mirror arrays can be applied e. g. for beam steering applications. Recently, UCLA presented a tip-tilt-piston micro mirror array with up to ±10° rotation and up to ±30 µm piston movement of the 1 mm diameter hexagonal shaped mirrors [24].

3.1 Subgrid adressing

Analog addressing also enables to tune the width of the intensity profile in the image plane. Let's assume that an optical set-up comprises a Fourier-filter allowing passing through the 0^{th} diffraction order, only. The intensity profile in the image plane is then defined by the undeflected mirrors. Mirrors deflected by λ/4 do not contribute intensity to the image plane (neglecting fringe effects). Figure 9 shows an example with the mirrors to the right and left are being deflected by λ/4. In the middle, three undeflected mirrors and a forth one (highlighted in red) are shown, the latter one being deflected by less than λ/4. When this red-highlighted mirror is stepwise deflected from 0 to λ/4 the width of the intensity profile is decreasing. The actual width of the intensity profile, for example defined by FWHM (full width half maximum) can thus be controlled by an amount less than defined by the pitch of the mirrors.

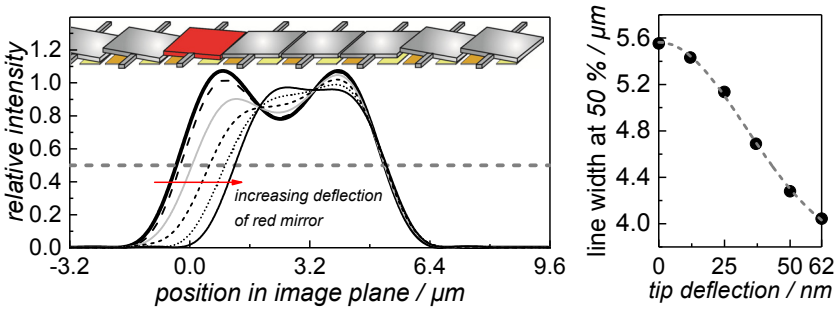

Figure 9. Subgrid addressing by partial deflection of the edge mirror. For a wavelength of 248 nm the deflection is varied between 0 and 62 nm. Pixel pitch is 16 µm. In the graph a demagnification by the optical set-up of 10x is assumed.

For example, the analog micro mirror devices of our group are applied for micro lithography applications at wavelengths down to 248 nm. For subgrid addressing mirror deflection is controlled with an accuracy of app. 1 nm allowing to achieve 63 grey values. With a micro mirror pitch of 16 µm and a demagnifying factor of 200, an addressing grid of 4 nm was achieved in the system (Mycronic AB).

3.2 Mirror planarity

In particular for high performance applications mirror planarity has significant impact on system performance especially with respect to the achievable contrast. Figure 10 shows the SEM image of a micro mirror array surface and the interferometrically determined surface profile. Such devices were developed for direct imaging of substrates for semiconductor packaging. The system, developed by Mycronic AB, provides a resolution of better than 10 µm lines and spaces. The micro mirror planarity is 1.5 nm RMS and is well within the specified range for the operation wavelength of 355 nm.

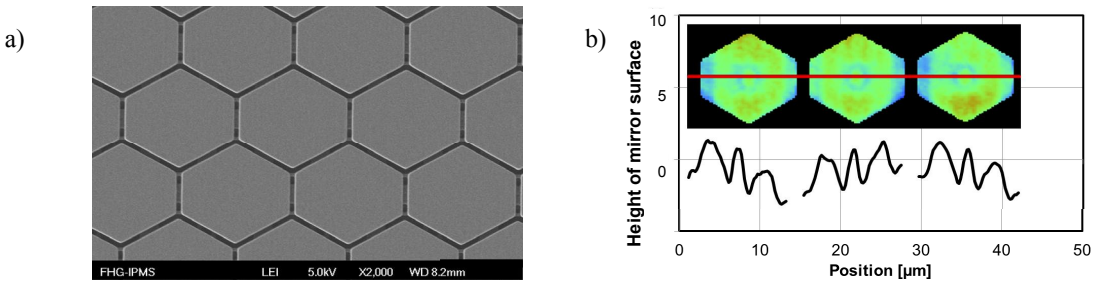

Figure 10. a) SEM image of the mirror surface. The hexagonal-shaped mirrors are suspended by buried, torsional hinges. b) Mirror topography determined by white light interferometry (RMS: 1.5 nm).

3.3 Irradiation resistance and high laser power operation

In particular DUV radiation can cause damage to the mirror plate surface, can motivate oxidation of addressing electrodes leading to charging effects and, in case of underlying electronic structures, also affect electronic functionality. The effect of the latter two can be decreased by high optical fill factor and suitable choice of the materials underneath the mirror plate. Purging the chip with nitrogen during operation avoids ozone-triggered oxidation. Results of our group prove that such measures are suitable to keep degradation and changes of materials underneath the mirror plate at a suitable low level. The dominant challenge towards processing very high laser energy densities is the irradiation resistance of the mirror plate surface. The two-level architecture of the mirror cell, with the mirror plate formed in the material layer of the upper level and the springs in the material layer of the lower level, allows us to independently optimize the respective materials regarding the mechanical and optical requirements. Several tests to investigate the influence of laser pulse rate, energy density and wavelength were performed. The bow of the mirror is a suitable parameter to evaluate the performance as it can be directly determined by white light interferometry. As an example, Figure 11 shows the change of the mirror bow due to illumination with an energy density about three orders of magnitude higher than that used for typical mask fabrication applications.

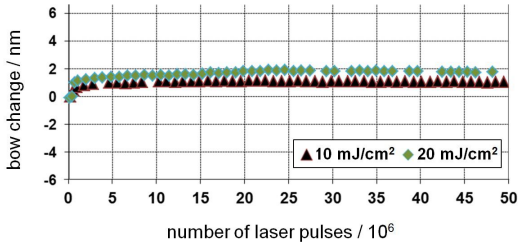

Figure 11. Typical result of an irradiation test of a device similar to that shown in Figure 8. The bow change (average of 500 mirrors) was monitored for 50 Mio. pulses at 10 and 20 mJ / cm² (λ = 248 nm, repetition rate: 1 kHz, pulse duration: app. 10 ns).

A 1D micro mirror array with 8192 addressable optical pixels, each consisting of 268 hexagonal mirrors (compare Figure 10) arranged in a line was developed for high speed modulation of the coherent light of a 355 nm diode-pumped solid state laser. Several tens of Watts are processed by the 4 x 82 mm² active area of the chip resulting in an average laser power density at the chip surface in the range of 10 W/cm².

Recently, our group further optimized mirror plate material, mirror cell design and also enhanced the optical device operation towards beam steering to support laser marking and engraving applications. Figure 12 shows an example of laser marking a CrNi-steel plate.

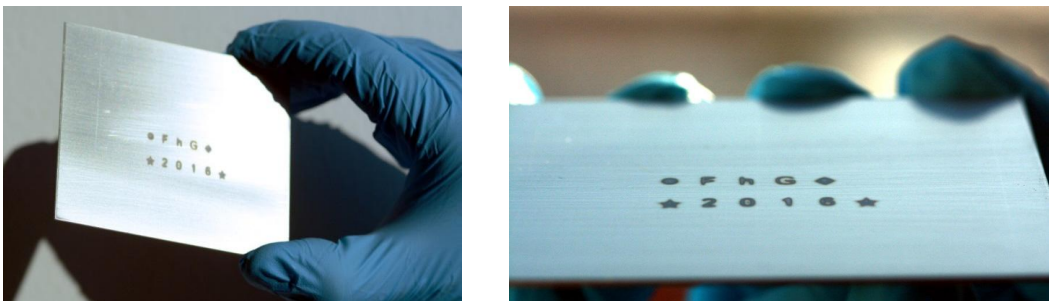

Figure 12. Beam steering micro mirror array based laser marking of a CrNi-steel plate. Energy density at the substrate: 0.6 up to 3.5 J/cm², wavelength: 248 nm.

4. SUMMARY

Several MOEMS devices for advanced imaging applications were presented. In general, MOEMS technology offers a large variety of solutions for applications requiring high-speed laser deflection and patterning, beam steering and image acquisition. Pixel rates of more than 100 Mpixels / s are supported by resonant scanning micro mirrors and more than 11 Gpixels / s by micro mirror arrays. The possibility to process laser intensities of several Watt encourages applications beyond laser displays and microlithography e. g. towards engraving and marking.

ACKNOWLEDGEMENTS

The authors thank all colleagues at Fraunhofer IPMS having contributed to the results. In particular, we want to thank Alexander Mai, Jan-Uwe Schmidt, Joerg Heber, Dirk Berndt, Thilo Sandner, Thomas Grasshoff and Christian Drabe. We also thank Michael Panzner from Fraunhofer IWS for the CrNi-steel plate engraving experiments. Mycronic AB, Sweden, is acknowledged for financing a large part of the presented micro mirror array development. Fraunhofer IPMS gratefully acknowledges financial sponsorship by the European Union within EU/FP7 project “PicoDiCon”.

REFERENCES

[1] Gu-Stoppel, S., Janes, J., Quenzer et al., "Two-dimensional scanning using two single-axis low-voltage PZT resonant micromirrors." Proc. SPIE 8977, MOEMS and Miniaturized Systems XIII, 897706. (2014).

[2] Wolter, A., Klose, T., Hsu, S.-T., Schenk, H., Lakner, H., "Scanning 2d micromirror with enhanced flatness at high frequency". Proc. SPIE 6114, MOEMS Display, Imaging, and Miniaturized Microsystems IV, 61140L. (2006).

[3] Sercalo, http://se055rz5.edis-lps.ch/products/pdfs/1mm3DegMEMS2DMIRROR.pdf (downloaded January 5, 2018).

[4] Schroedter, R., Roth, M., Janschek, K., Sandner, T., "Flatness-based open-loop and closed-loop control for electrostatic quasi-static microscanners using jerk-limited trajectory design", Mechatronics, http://dx.doi.org/10.1016/j.mechatronics.2017.03.005 (2017).

[5] Kenda, A., Kraft, M., Tortschanoff, W., Scherf, W. Sandner, T., Schenk, H. Lüttjohann, S., Simon, A., "Development, Characterization and Application of Compact Spectrometers based on MEMS with In-plane Capacitive Drives", Proc. SPIE Vol. 9101, 910102 (2014).

[6] Butschek , L., Hugger. S., Jarvis, J., Haertelt. M., Merten et al., „ Real-time Spectroscopy enabled by External Cavity QCLs with MOEMS Diffraction Gratings", Proc. SPIE Vol. 10111, Quantum Sensing and Nano Electronics and Photonics XIV; 101112G (2017).

[7] Mishra, K., van den Ende, D., Mugele, F., " Recent Developments in Optofluidic Lens Technology", Micromachines 2016, 102; DOI:10.3390/mi7060102 (2016).

[8] Bifano, T., "Adaptive imaging MEMS deformable mirrors", Nature Photonics, Vol. 5 (1) DOI: 10.1038/nphoton.2010.297 (2011).

[9] Texas Instruments, http://www.ti.com/product/DLP4710/datasheet/specifications#DLPS0511487 (downloaded January 10, 2018).

[10] Silicon Light Machines, http://www.siliconlight.com/wp-content/themes/siliconlight/pdf/8192-Channel-Integrated-GLV-Module.pdf (download January 10, 2018).

[11] Schmidt, J.-U., Dauderstaedt, U., Duerr, P., " High-speed one-dimensional spatial light modulator for Laser Direct Imaging and other patterning applications",Proc. SPIE Vol. 8977, 89770O, DOI: 10.1117/12.2036533 (2014).

[12] Sercalo, http://se055rz5.edis-lps.ch/products/pdfs/25x2mm4DegMEMS2DMIRROR.pdf (downloaded, January 5, 2018).

[13] Filhol, F., Defay, E., Divoux, C., Zinck, C., Delaye, M.-T., "Resonant micro-mirror excited by a thin-film piezoelectric actuator for fast optical beam scanning", Sensors and Actuators A, Vol. 123-124, pp. 483-489 (2005).

[14] Lemoptix, http://www.lemoptix.com/wp-content/uploads/2013/08/detailed-datasheet-mems-resonant-mirror-lemoptix.pdf (downloaded May 5, 2014).

[15] Kurth, S., Kaufmann, C., Hahn, R. et al., "A novel 24-kHz resonant scanner for high-resolution laser display. Proc. SPIE Vol. 5721, MOEMS Display and Imaging Systems III, No. 1, 23-33 (2005).

[16] Yalcinkaya, A. D., Urey, H., Holmstrom, "NiFe Plated Biaxial MEMS Scanner for 2-D Imaging". IEEE Photonics Technol. Lett., Vol. 19, No. 5, 330-332 (2007).

[17] Cho, J.-W., Park, Y.-H., Ko, Y.-C., Lee, B.-L., Kang, S.-J., Chung, S.-W., Choi, W.-K., Cho, Y.-C., Chang, S.-M., Lee, J.-H., Sunu, J., "Electrostatic 1D microscanner with vertical combs for HD resolution display", Proc. SPIE 6466, MOEMS and Miniaturized Systems VI, 64660B (2007).

[18] Baran, U., Brown, D., Holmstrom, S., Balma, D., Davis, W.O., Muralt, P., Urey, H., "Resonant PZT MEMS Scanner for High-Resolution Displays", J. Microelectromechanical Systems, Vol. 21, No. 6, 1303-1310 (2012).

[19] Drabe, Ch., Graßhoff, Th., Todt, U., Flemming, A., Sandner, T., Grahmann, J., "Scanning Optical MEMS with very high frequencies", 5th Laser Display and Lighting Conference (LDC'16), Jena, Germany, July, 4th - 8th (2016).

[20] Hsu, S.-T., Klose, T., Drabe, C., Schenk, H., "Fabrication and characterization of a dynamically flat high resolution micro-scanner", J. Opt. A: Pure Appl. Opt. 10, Vol. 10, 044005, pp. 1-8 (2008).

[21] Wang, Y., Wu, M. C., "Micromirror based optical phased array for wide-angle beamsteering", IEEE MEMS, Las Vegas (2017).

[22] Texas Instruments, http://www.ti.com/lit/ds/dlps024b/dlps024b.pdf (downloaded May 11, 2014).

[23] Texas Instruments, http://www.ti.com/product/DLP660TE (downloaded January 6, 2018).

[24] Hopkins, J. B., Panas, R. M., Song, Y., White, C. D., "A High-Speed Large-Range Tip-Tilt-Piston Micromirror Array", J. Micromech. Systems, Vol. 26, No. 1 (2017).

[25] Mai, A. Bunce, C., Hübner, R., Pahner, D., Dauderstädt, U. "In situ bow change of Al-alloy MEMS micromirrors during 248-nm laser irradiation," J. Micro/Nanolith. MEMS MOEMS 15(3), 035502 (2016).